A Novel Method to Increase Tumor Ablation Zones With RFA by Injecting the Cationic Polymer Solution to Tissues: *In Vivo* and Computational Studies

Zheng Fang, Michael A. J. Moser, Edwin M. Zhang, Wenjun Zhang, *Senior Member, IEEE*, and Bing Zhang, *Member, IEEE*

***Abstract*—*Objective*: This study aims to examine, for the first time, the introduction of cationic polymer solutions to improve radiofrequency ablation (RFA) in terms of a potentially enlarged ablation zone. *Methods*: By using *in vivo* and computational RFA studies, two cationic polymers, Chitooligosaccharides (COS) and carboxymethyl chitosan (CMC), diluted in deionized water, were injected into tissues separately surrounding the RF bipolar electrode prior to power application. A total of 9 rabbits were used to 1) measure the increase in electrical conductivity of tissues injected with the cationic polymer solutions, and 2) explore the enhancement of the ablation performance in RFA trials. A computer model of RFA comprising a model of the solution diffusion with an RF thermal ablation model was also built, validated by the *in vivo* experiment, to quantitatively study the effect of cationic polymer solutions on ablation performances. *Results*: Compared to the control group, the electrical conductivity of rabbit liver tissues was increased by 42.20% (0.282 $\pm$ 0.006 vs. 0.401 $\pm$ 0.048 S/m, $P = 0.001$) and 43.97% (0.282 $\pm$ 0.006 vs. 0.406 $\pm$ 0.042 S/m, $P = 0.001$) by injecting the COS and CMC solution at the concentration of 100 mg/mL into the tissues, denoted COS_{DW100} and CMC_{DW100}, respectively. Consequently, the *in vivo* experiments show that the ablation zone was enlarged by 95% (47.6 $\pm$ 6.3 vs. 92.6 $\pm$ 11.5 mm^2, $P < 0.001$) and 87% (47.6$\pm$ 6.3 vs. 88.8 $\pm$ 9.6 mm^2, $P < 0.001$) by COS_{DW100} and CMC_{DW100}, respectively. The computer simulation shows that the ablation zone was enlarged by 71% (51.9 vs. 88.7 mm^2) and 63% (51.9 vs. 84.7 mm^2) by COS_{DW100} and CMC_{DW100}, respectively. *Conclusion*: The injection of the cationic solution can greatly improve the performance of RFA treatment in terms of enlarging the ablation zone, which is due to the increase in the electrical conductivity of liver tissues surrounding the RF electrode. *Significance*: This study contributes to the improvement of RFA in the treatment of large tumors.**

***Index Terms*—Radiofrequency ablation, computer model, *in vivo* experiment, tumor ablation enhancement, cationic polymer solution.**

I. Introduction

RADIOFREQUENCY ablation (RFA) as a thermal ablation therapy is extensively used to treat primary and secondary malignancies in clinical practice [1], [2]. During RFA treatments, ions and electrons inside biological tissues move forward and backward rapidly driven by an alternating current (375–500 kHz) to generate the friction-induced heat for heating tissues to 50–100 °C [3]. However, when the tissue is heated above 100 °C, it becomes desiccated due to water evaporation and further charred. In fact, the RFA systems currently used in clinical practice are designed such that the delivery of RF power is halted when an abrupt increase in impedance has been detected, a phenomenon known as "roll off" [4], [5]. Roll-off due to increased impedance is one of the main reasons for the incomplete ablation of large tumors treated by RFA.

Such phenomenon has motivated several efforts in various areas to get around this "roll off" problem, ranging from RF electrode design to target tissue property modification. The cool-tip electrode is used to cool tissue temperature around the electrode, which has the effect of delaying tissue charring in clinical practice [6]. Fang *et al*. proposed a novel expandable electrode to re-distribute electric field for avoiding roll-off [7], [8]. Zhang *et al*. proposed a novel feedback control method to avoid roll-off by controlling RF power delivery [9]. Meanwhile, other authors have demonstrated that the injection of normal saline solution or diluted hydrochloric acid (HCl) can efficiently delay roll-off

Manuscript received August 20, 2019; revised September 16, 2019; accepted October 10, 2019. Date of publication October 15, 2019; date of current version May 20, 2020. This work was supported in part by 111 Project (D18003), in part by the National Natural Science Foundation of China under Grants 81801795 and 61873158, and in part by the Natural Science Foundation of Shanghai under Grant18ZR1415100. *(Corresponding authors: Wenjun Zhang; Bing Zhang.)*

Z. Fang is with the School of Mechanical and Power Engineering, East China University of Science and Technology.

M. A. J. Moser is with the Department of Surgery, University of Saskatchewan.

E. M. Zhang is with the Division of Vascular & Interventional Radiology, Department of Medical Imaging, University of Toronto.

W. Zhang is with the School of Mechanical and Power Engineering, East China University of Science and Technology, Shanghai 200237, China, and also with the Division of Biomedical Engineering, University of Saskatchewan, Saskatoon, SK S7K 5A9, Canada (e-mail: chris.zhang@usask.ca).

B. Zhang is with the Energy-based Tumor Ablation Laboratory, School of Mechatronic Engineering and Automation, Shanghai University, Shanghai, China (e-mail: bingzhang84@shu.edu.cn).

This paper has supplementary downloadable material available at http://ieeexplore.ieee.org, provided by the authors.

Digital Object Identifier 10.1109/TBME.2019.2947292

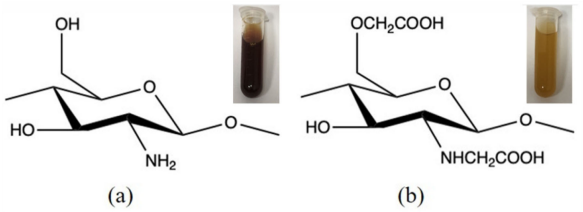

Fig. 1. Molecular structures of (a) COS and (b) CMC. The top-right is the corresponding solution dissolved in deionized water.

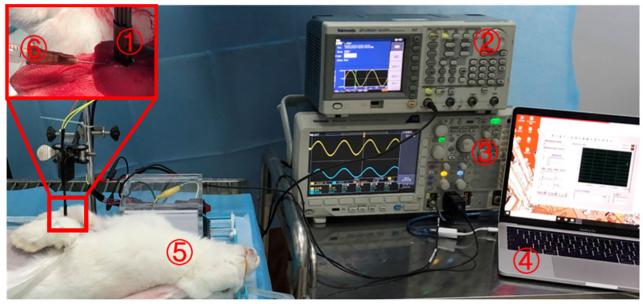

Fig. 2. Electrical conductivity measurement system: (1) the four-electrode device, (2) the power source, (3) the oscillography for measuring current and voltage, (4) the software for data collection and calculation, (5) New Zealand white rabbit, and (6) the injection of solution.

occurrence and lead to achieving larger ablative zones [10], [11]. It is commonly recognized that the injection of saline solution changes the electrical conductivity to allow more RF energy deposition and improves the thermal conduction within the tissues by rapidly convecting heat over a large tissue volume [12]. In addition, the injected solution can cool the tissues down, which also can delay tissue charring and roll-off and lead to larger ablation zones. However, there are some limitations accompanying this approach, especially over large volumes. Because it is difficult to achieve uniform fluid diffusion and distribution of saline solution, the improved electrical conductivity is inherently non-uniform, leading to undesired or irregular tumor ablation enlargements [13].

In the present study, instead of saline solution, two cationic polymers, chitooligosaccharides (COS) and carboxymethyl chitosan (CMC) (Fig. 1), were proposed, for the first time, to be used in RFA to alter the electrical conductivity of biological tissues for achieving larger ablation zones. The electrical conductivity of tissues can be improved by COS or CMC solution similarly to saline solution due to the migration of ions in the solution and the polarization in the alternating field [14]. Both COS and CMC are derived from chitosan, which is a biocompatible and biodegradable natural polymer, and they are soluble in water.

There are other potential benefits to using these polymers: They are reported to have antibacterial and anti-infective effects [15]–[17]. Also, both COS and CMC may have an inhibitory effect on tumor growth and metastasis with low or no systematic toxicity [18]–[20]. For example, Shen *et al*. [18] demonstrated the inhibitory effect on tumor growth and metastasis of fungal-derived COS for both HepG2 tumor and Lewis lung carcinoma metastasis. Meanwhile, Jiang *et al*. [19] showed that the polymers lead to an inhibition of MMP-9, VEGF, and E-selection expression. Finally, COS and CMC are each able to be used as a carrier in drug or gene delivery and protein transferring [17], [21], [22]. It is noteworthy that, due to the higher dynamic viscosity, the cationic polymer solution can be more easily measured in terms of better diffusion and distribution performance than the saline solution [23], [24]. Thus, the cationic polymer is a potentially effective surfactant for enhancing the tumor ablation zones with RFA. Meanwhile, the immune-enhancing activity of COS or CMC may further ensure the complete ablation avoiding tumor-recurrence [25], [26].

The electrical conductivity of rabbit liver tissues injected with COS or CMC solution was measured *in vivo* using the four-electrode method in this study [27]. A three-dimensional computer model validated by the *in vivo* experiment was used to study the improved performance of RFA with the cationic polymer solutions.

II. *In Vivo* Experiment

All *in vivo* experiments were performed at the Shanghai Jambo Biological Technology laboratory with the approval for these trials from the Institution of Shanghai Science and Technology Commission. All operations were in accordance with the general guidelines issued by the Institute of Zoology, Chinese Academy of Science. A mixed solution of 0.15–0.2 ml/kg (Zoletil 50 and Lumianning with a ratio of 5:2) was used as the pre-operative anesthesia. After the experiment, an overdose of injection anesthesia was performed for the euthanasia of animals.

A. Measurement of Electrical Conductivity

In this study, deionized water (DW) was used to dissolve COS or CMC leading to the cationic polymer solution, denoted as COS_{DW} and CMC_{DW}, respectively. As shown in Fig. 2, the electrical conductivity of rabbit liver tissues injected with three concentrations of COS_{DW} or CMC_{DW} was measured *in vivo* for studying the enhancing effect by a custom-made four-electrode system, and each concentration was performed in quintuplicate. The number subscript denotes the concentration of cationic polymer solutions in DW; for instance, COS_{DW10} means the concentration of COS solution is 10 mg/mL; three different concentrations of cationic solutions (i.e., COS_{DW10}, COS_{DW50}, and COS_{DW100}) were used in the study. The four-electrode systems used to measure electrical conductivity included: (1) a custom-made four-electrode device [27], (2) a function generator (AFG3022C, Tektronix, Beaverton, Oregon, USA) supplying a 500 kHz and 0.1-3 mA alternating current, (3) an oscilloscope (MDO 3032, Tektronix, Beaverton, Oregon, USA) measuring the current via a current probe (CT-2 current probe, Tektronix, Beaverton, Oregon, USA) and the voltage via a voltage probe (TPP0500B, Tektronix, Beaverton, Oregon, USA), and (4) a software for data collection and calculation A total of six New Zealand rabbits (2.8-3.4 kg) with three lobes

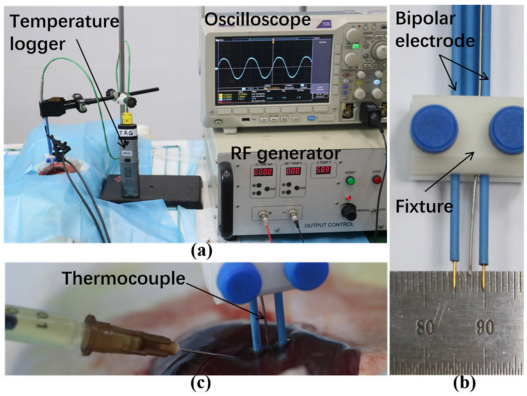

Fig. 3. *In vivo* experiment: (a) RFA administration, (b) the injection of solution, and (c) bipolar gold-tip electrode.

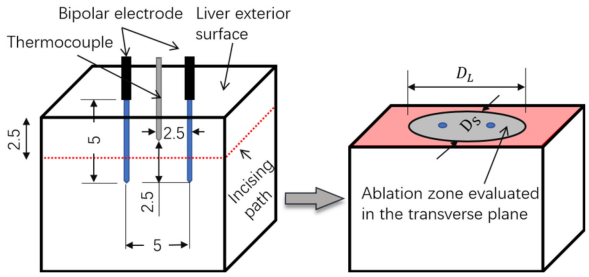

Fig. 4. *In vivo* ablation zone evaluation of treated liver samples (Unit: mm).

each were used in the measurement, and each lobe of rabbit livers was used once or twice depending on the size of lobes. At least 0.5 mL of cationic polymer solution at each concentration was injected into the liver lobe to ensure that the area of interest was well infiltrated with solution. the interested site was fully filled with the solution. The measurement was immediately performed after solution injection.

B. RFA Setting and Ablation Experiments

The enhancement of RFA using the cationic polymer solution was studied by an *in vivo* experiment using a rabbit liver model. A custom-made RF power generator (500 kHz and 200 W) was used in the RFA experiment (Fig. 3a). A commercially-available bipolar gold-tip electrode (Genetrode, 508, Harvard Apparatus, Holliston, MA, USA) with a center-to-center distance of 5 mm and an insert depth of 5 mm was used to apply the RF energy (Fig. 3b). Meanwhile, a thermocouple was used to measure the temperature at the central point between two electrodes with an insertion depth 2.5 mm, and the temperature data was collected by a temperature logger (SSN-61, YuWen inc., Shenzhen, China), as shown in Fig. 3a. Three New Zealand white rabbits (3.1-3.4 kg) with three liver lobes each were used in the study and randomly divided into three groups based on the injected solutions: control group (no solution injection), $\mathrm{COS}_{\mathrm{DW100}}$ group, and $\mathrm{CMC}_{\mathrm{DW100}}$ group. The $\mathrm{COS}_{\mathrm{DW100}}$ and $\mathrm{CMC}_{\mathrm{DW100}}$ were ultraviolet sterilized before the injection. Then, 0.2 mL of solution was injected at the middle of each RF bipolar electrode before RF power application (Fig. 3c). After the solution was injected, a constant current (0.06 A) was delivered immediately, and the value of current was monitored and adjusted in real time by the oscilloscope (Fig. 3a). The criterion of the termination of RFA procedure is roll-off occurrence (i.e., the supplied current decreased sharply and was less than 10 mA). Each *in vivo* RFA trial was performed in quadruplicate, with each lobe of rabbit liver receiving one or two RFA treatments, depending on the sizes of lobes and ablation zones.

Each animal was then euthanized and the treated liver sample was retrieved and sectioned immediately. As shown in Fig. 4, the ablation zone was evaluated in the transverse plane, which is perpendicular to the bipolar electrode. The "white zone" (corresponding to protein denaturation) was measured to provide two parameters for each treatment zone: long diameter (D_L) and short diameter (D_S). The area (S) and roundness (R) of ablation zone were also examined and calculated by $\cdot S = \pi D_L \cdot D_S/4$ and $R = D_S/D_L$, respectively.

C. Statistical Analysis

All results were given as mean $\pm$ standard deviation (SD). A one-way analysis of variance (ANOVA) were used to assess for a statistically significant difference in the results of all experiments using SPSS software (SPSS statistics 24, IBM Inc, Armonk, NY, USA). The Bonferroni method was used adjust for multiple comparisons [28]. Results were considered statistically significant for $P < 0.05$.

III. Computational Modeling

A. Solution Diffusion Model

A solution diffusion model was used in this study to simulate the process of cationic solution diffusion into the liver tissues. The velocity of solution in the tissues was described by Darcy's law:

$$u = -\frac{\kappa}{\mu} \cdot \nabla p \tag{1}$$

where p is the pressure, κ is the permeability, and μ is the dynamic viscosity of solution. Further, the continuity equation for steady-state incompressible flow was given by [29], [30]

$$\nabla u_i = \Theta_v - \Theta_L \tag{2}$$

$$\nabla u_v = \Theta_v \tag{3}$$

where Θ_v is solution source term between the interstitium and vasculature based on Starling's law, and Θ_L is the lymphatic drainage term, which is non-negative term meaning there is no backflow of solution from lymphatic into interstitium. These two values can be given by

$$\Theta_v = \frac{L_{p,v} S_v}{V} \left[p_v - p - \sigma_t \left(\pi_v - \pi_i \right) \right] \tag{4}$$

$$\Theta_L = \max \left(\frac{L_{p,L} S_L}{V} \left(p - p_L \right), 0 \right) \tag{5}$$

where L_p is the hydraulic conductivity, S/V is the surface area per unit volume, π is the osmotic pressure, and σ_t is the osmotic reflection coefficient; the subscript '*v*', '*i*', and '*L*' represent vasculature, interstitium, and lymphatics, respectively.

In addition, the solution concentration distribution inside the tissues was described by the convection-diffusion equation for the interstitium and vasculature, by Eq. (6) and Eq. (7), respectively [30], [31]

$$\frac{\partial c_i}{\partial t} + \nabla \cdot (-D\nabla c_i) + v_i \cdot \nabla c_i = \frac{F_L - F_s}{w_i} \tag{6}$$

$$\frac{\partial c_v}{\partial t} + \nabla \cdot (-D\nabla c_v) + v_v \cdot \nabla c_v = \frac{F_s}{w_v} \tag{7}$$

where c is the solution concentration in the tissue, D is the solution diffusion coefficient in the tissue, which was assumed as saline in the study, $v = u/\varepsilon$ is the actual solution velocity considering the porosity ε, and F_s is the source term describing the solute transport between the vasculature and interstitium, given by

$$F_s = \Theta_v (1 - \sigma_f) \frac{c_v - c_i}{2} + \frac{P_w S_v}{V} (c_v - c_i) \tag{8}$$

where, σ_f is the solute retardation coefficient, and P_w is the permeability of blood vessel wall. Similarly, F_L is the source term describing the solute transport between the lymphatics and interstitium, described by

$$F_L = \Theta_L c_i \tag{9}$$

B. Thermal Ablation Model

RFA procedure was described by using the Penne's bio-heat transfer equation [32]

$$\rho c_p \frac{\partial T(\boldsymbol{x}, t)}{\partial t} = \nabla \cdot k \nabla T(\boldsymbol{x}, t) + \rho_b c_{pb} \omega_b (T_b - T(\boldsymbol{x}, t)) + Q_{hs}(\boldsymbol{x}, t) + Q_m(\boldsymbol{x}, t) \quad \boldsymbol{x} \in \Lambda \tag{10}$$

where ρ is the density, c_p is the specific heat, $T(\boldsymbol{x}, t)$ is the temperature, k is the thermal conductivity, ρ_b is the blood density, c_{pb} is the specific heat of the blood, ω_b is the blood perfusion, T_b is the temperature of the blood entering the tissue assumed to be 37 °C, $\boldsymbol{x} = \{x,\ y,\ z\}$ in the Cartesian coordinate system, $\wedge$ denotes the analyzed spatial domains, $Q_m(\boldsymbol{x}, t)$ is the energy generated due to metabolic processes which has been neglected since metabolic heat source is magnitude less than the spatial heat, and $Q_{hs}(\boldsymbol{x}, t)$ generated by the *RF* electrical current as follows [33]

$$Q_{hs} = \boldsymbol{J} \cdot \boldsymbol{E} = \sigma |\nabla U|^2 \tag{11}$$

where $\boldsymbol{J}$ is the current density, $\boldsymbol{E}$ is the electrical field intensity, σ is the electrical conductivity, and U is the applied voltage.

All values of the physical properties in the model were tabulated in the Table I, and the dynamic viscosities of $\mathrm{COS_{DW100}}$ and $\mathrm{CMC_{DW100}}$ were measured by a rheometer (HAAKE Mars III, Thermo Fisher Scientific Inc., Waltham, MA, USA). The temperature-dependent varieties of thermal conductivity and electrical conductivity of liver tissue at the temperature below 100 °C were defined by the following equations [5], [34]:

TABLE I
PHYSICAL PROPERTIES OF THE MATERIALS USED IN THE MODEL

Parameter	Value	Ref.
Diffusion model		
Solution density for $\mathrm{COS_{DW100}}$, ρ_1 (kg/m^3)	1040	18 °C
Solution density for $\mathrm{CMC_{DW100}}$, ρ_2 (kg/m^3)	1047	18 °C
Diffusion coefficient for the interstitum, D_i (m^2/s)	1×10^{-9}	[29]
Diffusion coefficient for the vasculature, D_v (m^2/s)	4.2×10^{-10}	[29]
Dynamic viscosity of COS, μ_1 (Pa·s)	0.02±0.02	37 °C
Dynamic viscosity of CMC, μ_2 (Pa·s)	0.38±0.25	37 °C
Interstitial space permeability, κ_i (m^2)	3.12×10^{-17}	[31]
Vascular space permeability, κ_v (m^2)	1.56×10^{-14}	[31]
Vasculature hydraulic conductivity, $L_{p,v}$ (m/(Pa·s))	2.7×10^{-12}	[31]
Vascular surface area to volume ratio, S_v/V (m^{-1})	7000	[29]
Lymphatics transfer coefficient, $L_{p,L}S_L/V$ (Pa·s)$^{-1}$	4.43×10^{-9}	[31]
Lymphatics pressure, p_L (Pa)	133.3	[31]
Vascular osmotic pressure, π_v (Pa)	2666.67	[31]
Interstitial fluid osmotic pressure, π_i (Pa)	1333.33	[31]
Osmotic reflection coefficient, σ_t	0.91	[31]
Permeability of blood vessel wall, P_w (m/s)	7.3×10^{-10}	[30]
Solute retardation coefficient, σ_f	0.9	[31]
Volume fraction of interstitial space, w_i	0.857	[31]
Volume fraction of vascular space, w_v	0.143	1-w_i
Tissue porosity, ε_i	0.6	[31]
Vascular porosity, ε_v	1	[31]
Electrical model		
Slope for COS, λ_1 ((S·m^2)/kg)	1.19×10^{-3}	37 °C
Slope for CMC, λ_2 ((S·m^2)/kg)	1.24×10^{-3}	37 °C
Liver electrical conductivity, σ_0 (S/m)	0.282	37 °C
Electrode electrical conductivity, σ_e (S/m)	1×10^{8}	[36]
Thermal model		
Liver density, ρ_l (kg/m^3)	1080	[37]
Liver specific heat, c_p (J/(kg·K))	3455	[37]
Liver thermal conductivity, k_0 (W/(m·K)	0.563	[34]
Electrode density, ρ_e (kg/m^3)	6450	[38]
Electrode specific heat, c_{pe} (J/(kg·K))	840	[38]
Electrode thermal conductivity, k_e (W/(m·K))	18	[38]
Blood density, ρ_b (kg/m^3)	1000	[38]
Blood specific heat, c_{pb} (J/(kg·K))	4180	[38]
Blood thermal conductivity, k_b (W/(m·K)	0.49	[38]
Blood perfusion rate, ω_{b0} (1/s)	0.042	[39]
Heat transfer coefficient, h (W/(m^2·K))	100	[40]
Cell death model		
Frequency factor, A (1/s)	7.39×10^{39}	[37]
Activation energy, ΔE (J/mol)	2.577×10^{5}	[37]

$$k(T) = k_0 + 0.002601 (T(\boldsymbol{x}, t) - T_0) \tag{12}$$

$$\sigma(T) = \sigma(c) [1 + 0.02 (T(\boldsymbol{x}, t) - T_0)] \tag{13}$$

$$\sigma(c) = \lambda \cdot c + \sigma_0 \tag{14}$$

where k_0 and σ_0 are the constant thermal conductivity and electrical conductivity, respectively, at the reference temperature (T_0 = 37 °C). At the temperature above 100 °C, a constant value at the temperature of 100 °C of the thermal conductivity was taken. The electrical conductivity decreases by 2 orders of magnitude from 100 to 105 °C and, then, was kept as a constant. $\sigma(c)$ is the enhanced electrical conductivity by COS or CMC, which is determined by Eq. (14). c is the concentration of COS or CMC. σ_0 is the baseline electrical conductivity (σ_0) of rabbit liver (at T_0 = 37 °C). λ is the slope of the linear function between $\sigma(c)$ and c, which is predicted by the *in vivo* measurement results of $\sigma(c)$. In addition, the blood perfusion of rabbit liver was simulated by the piecewise function [32]

$$\omega_b(t) = \begin{cases} \omega_{b0} & \text{for } T \le 50\,^\circ\mathrm{C} \\ 0 & \text{for } T > 50\,^\circ\mathrm{C} \end{cases} \tag{15}$$

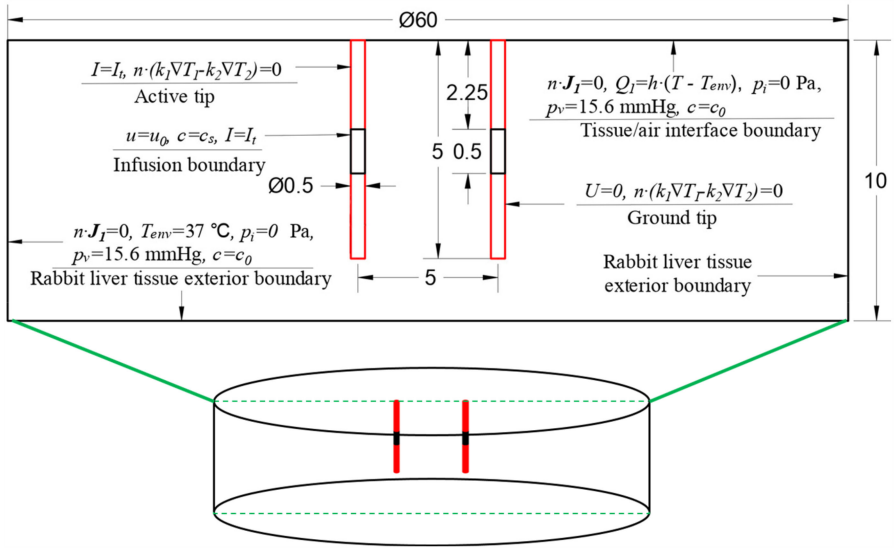

Fig. 5. Dimension (out of scale and in mm) of the 3D *in vivo* liver RFA model with a slice showing boundary conditions.

where ω_{b0} (1/s) is the constant blood perfusion of rabbit liver tissue.

Then, the induced thermal damage was evaluated by the Arrhenius model for the estimation of ablation zones [35]

$$\Omega(t) = A\int_0^t e^{\frac{-\Delta E}{RT(\tau)}}d\tau \tag{16}$$

where A is the frequency factor, ΔE is the activation energy barrier, R is the universal gas constant $(8.314\,\mathrm{J\,mol^{-1}K^{-1}})$. The threshold of tissue death is $\Omega(t) \geq 4.6$, which means a 99% probability of cell death.

C. Boundary Conditions

As shown in Fig. 5, a three-dimensional finite element RFA model was used to simulate the *in vivo* RFA experiment. A cylinder with the diameter of 60 mm and the height of 10 mm was used to model the liver tissues. Two small cylinders with 0.5 mm in diameter and 5 mm in length were set as the bipolar electrode; one was taken as the ground pad and the other supplying a constant RF current (0.06 A) as the active tip during RFA procedure. Considering 1) the relatively small size of injection hole (syringe needle) compared to injected solution volume and tissue volume, and 2) computational cost and convergence, a cylindrical infusion boundary (i.e., $u = u_0$) was set at the middle of each electrode (the black part) for mimicking the solution injection via the syringe needle, as shown in Fig. 5. In accordance with the *in vivo* experiment, the inlet velocity (u_0) was set as 2.55×10^{-2} m/s, which was defined by the actual injection solution volume (0.2 mL for each electrode), the injection time (10 s), and the area of infusion boundary. The body temperature of 37 °C was set as the initial temperature of this model, and Dirichlet boundaries were set at the outer surfaces of tissue ($T = 37$ °C, $p = 0$ Pa and $c = 0$ mg/mL). Meanwhile, a Robin heat-transfer boundary was set at the upper surface $(Q = h(T - T_{env}))$, which is the interface between tissue and air, and the environment temperature (T_{env}) was set at the room temperature (15 °C). The initial concentration was set as $c_0 = 0$ mg/mL in the model, corresponding the absence of COS or CMC solution in the tissue initially. Then, other boundary conditions were set.

D. Mesh Convergence Test

COMSOL Multiphysics 5.3a software (COMSOL Inc., Burlington, MA, USA) was used to simulate *in vivo* RFA procedure with the injection of COS and CMC solution. The mesh convergence criterion was considered as the difference in the maximum temperature between two contiguous meshes smaller than 0.1%. Eventually, the element number of 61965 was used in the model. In detail, the whole geometry domain contains three parts: part I is the bipolar electrode, part II is a cylindrical domain (12 mm in diameter) which is the main temperature changing zone, and part III is the remaining parts of model. For the part I, an extra fine swept way was used to discretize the geometry domain. Then, the free tetrahedral mesh was used to discretize the part II and III, and the mesh of part II and III were fixed at the default "Extra fine" and "Normal" in COMSOL, respectively.

IV. Results

A. Electrical Conductivity

The electrical conductivity of $\mathrm{COS_{DW}}$ or $\mathrm{CMC_{DW}}$ was measured before RFA experiments, as shown in Fig. 6. $\mathrm{CMC_{DW10}}$ has lower electrical conductivity than $\mathrm{COS_{DW10}}$ (0.298 ± 0.006 vs. 0.35 ± 0.006 S/m, $P = 0.004$). However, at a concentration of 50 or 100 mg/ml, $\mathrm{CMC_{DW}}$ presents a higher electrical conductivity than $\mathrm{COS_{DW}}$ (1.7 ± 0.008 vs. 1.534 ± 0.033, $P = 0.031$ and 2.862 ± 0.019 vs. 2.474 ± 0.02 S/m, $P = 0.223$, respectively). Meanwhile, both $\mathrm{COS_{DW}}$ and $\mathrm{CMC_{DW}}$ have significant increases in the electrical conductivity as an increase in the concentration of cationic polymer (both $P < 0.001$).

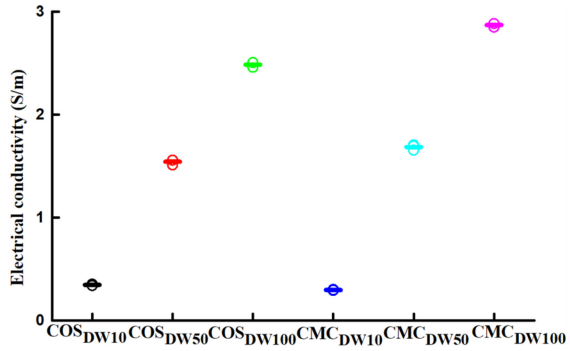

Fig. 6. Electrical conductivity of COS and CMC in deionized water.

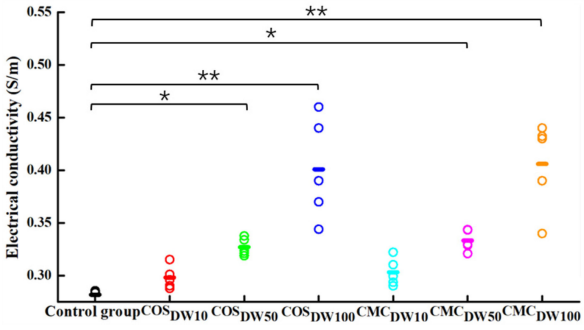

Fig. 7. Electrical conductivity of rabbit livers injected with different concentration COS and CMC solution. The average value was shown as dash line. $*P < 0.05$, $**P < 0.001$.

As shown in Fig. 7, the electrical conductivity of rabbit liver tissues injected with $\mathrm{COS_{DW}}$ or $\mathrm{CMC_{DW}}$ was increased significantly at all concentrations of cationic polymer solutions except $\mathrm{COS_{DW10}}$ and $\mathrm{CMC_{DW10}}$. Specifically, the electrical conductivity was increased by 15.96% (0.282 ± 0.006 vs. 0.327 ± 0.008 S/m, $P = 0.017$) and 42.20% (0.282 ± 0.006 vs. 0.401 ± 0.048 S/m, $P < 0.001$) by introducing $\mathrm{COS_{DW50}}$ and $\mathrm{COS_{DW100}}$, respectively. Correspondingly, by introducing $\mathrm{CMC_{DW50}}$, and $\mathrm{CMC_{DW100}}$, the conductivity was increased by 18.09% (0.282 ± 0.006 vs. 0.333 ± 0.010 S/m, $P = 0.004$), and 43.97% (0.282 ± 0.006 vs. 0.406 ± 0.042 S/m, $P < 0.001$), respectively.

B. In Vivo RFA Experiment Results

$\mathrm{COS_{DW100}}$ and $\mathrm{CMC_{DW100}}$, which have highest electrical conductivities among the solutions with the different concentrations, were used in the *in vivo* experiments. As shown in Fig. 8, compared to control group, a marked enlargement in the ablation zone was recognized in both $\mathrm{COS_{DW100}}$ and $\mathrm{CMC_{DW100}}$ groups, but there was no significant difference in the ablation zone between $\mathrm{COS_{DW100}}$ group and $\mathrm{CMC_{DW100}}$ group. For details, by injecting $\mathrm{COS_{DW100}}$ and $\mathrm{CMC_{DW100}}$,D_L was increased by 24% (9.48 ± 0.57 vs. 11.75 ± 0.76 mm, $P = 0.011$) and 23% (9.48 ± 0.57 vs. 11.68 ± 0.76 mm, $P = 0.013$), respectively, and D_S was increased by 56% (6.38 ± 0.53 vs. 9.95 ± 0.71 mm, $P < 0.001$) and 52% (6.38 ± 0.53 vs. 9.68 ± 0.24 mm, $P < 0.001$), respectively. A similar increase was also found in both the ablation time (T_a) and the roundness (R) of ablation zone (Fig. 9b, 9c). The ablation time was increased from 77 ± 17 s to 300 ± 104 s and 275 ± 73 s because of the introduction of $\mathrm{COS_{DW100}}$ and $\mathrm{CMC_{DW100}}$, respectively. In other words, the roll-off was significantly delayed, allowing greater RF energy deposition in $\mathrm{COS_{DW100}}$ or $\mathrm{CMC_{DW100}}$ group. It is noteworthy that the shape of ablation zones was also improved in the two cationic solution groups. We believe that one of the major reasons causing this improvement is the local tissue electrical conductivity enhancement around the electrodes, which decreases the energy deposition near the electrodes delaying the roll-off occurrence. The end result was that the injection of $\mathrm{COS_{DW100}}$ and $\mathrm{CMC_{DW100}}$ led to a 95% increase in the size of the ablation zone (47.6 ± 6.3 vs. 92.6 ± 11.5 mm^2, $P < 0.001$) and 87% (47.6 ± 6.3 vs. 88.8 ± 9.6 mm^2, $P < 0.001$), respectively, but there was no significant difference between the cationic solution groups ($P = 1$) (Fig. 9d).

C. In Vivo RFA Simulation Results

As shown in Fig. 10, a spherical cationic solution diffusion shape was found for both $\mathrm{COS_{DW100}}$ and $\mathrm{CMC_{DW100}}$ at the final injection time. Diffusion shape was found to be quite regular and round, which is more predictable. The difference in the distribution area between these two cationic solutions was found to be negligible. The diameter of the concentration greater than 50 mg/mL are 6.9 and 6.6 mm for $\mathrm{COS_{DW100}}$ and $\mathrm{CMC_{DW100}}$, respectively (the zone inside the black circle in Fig. 10a–b has a concentration of greater than 50 mg/mL of the polymer). In addition, it is noteworthy that a ring-like solution distribution was found in $\mathrm{CMC_{DW100}}$. A possible reason causing this phenomenon is due to the higher dynamic viscosity of $\mathrm{CMC_{DW100}}$, which increased the pressure at the solution injection site. More $\mathrm{CMC_{DW100}}$ solution was pushed away from the electrode as a ring-like structure.

Further, the introduction of $\mathrm{COS_{DW100}}$ or $\mathrm{CMC_{DW100}}$ also has remarkable influences on the tissue impedance, temperature and potential distribution, and ablation time. Compared to control group, the minimum impedance during the RFA procedures was decreased by 23% (311 vs. 238 Ω) for $\mathrm{COS_{DW100}}$ and 23% (310 vs. 237 Ω) for $\mathrm{CMC_{DW100}}$. As shown in Fig. 11, the ablation time (T_a) was also increased by 335% (72 vs. 313 s) for $\mathrm{COS_{DW100}}$ and 275% (72 vs. 270 s) for $\mathrm{CMC_{DW100}}$. Fig. 12 shows the temperature distribution in the transverse plane following the incising path and the temperature history of central point of transverse plane. The highest temperature at the central point of transverse plane was 92.5, 92.2, and 92.0 °C for control, $\mathrm{COS_{DW100}}$ and $\mathrm{CMC_{DW100}}$ groups, respectively, showing that a more uniform temperature distribution can be achieved by using cationic polymer solutions. Similarly, a larger zone where the temperature exceeded 50 °C, (depicted by the black circles in Fig. 12g and k) was achieved in the $\mathrm{COS_{DW100}}$ or $\mathrm{CMC_{DW100}}$ group. In addition, electrical conductivity and potential distributions are available as Supplementary Fig. 1 and Fig. 2, respectively, accompanying the online article.

Finally, Table II and Fig. 13 shows the simulation results, and all results (i.e., D_L, D_S, S, T_a, and R) located in the

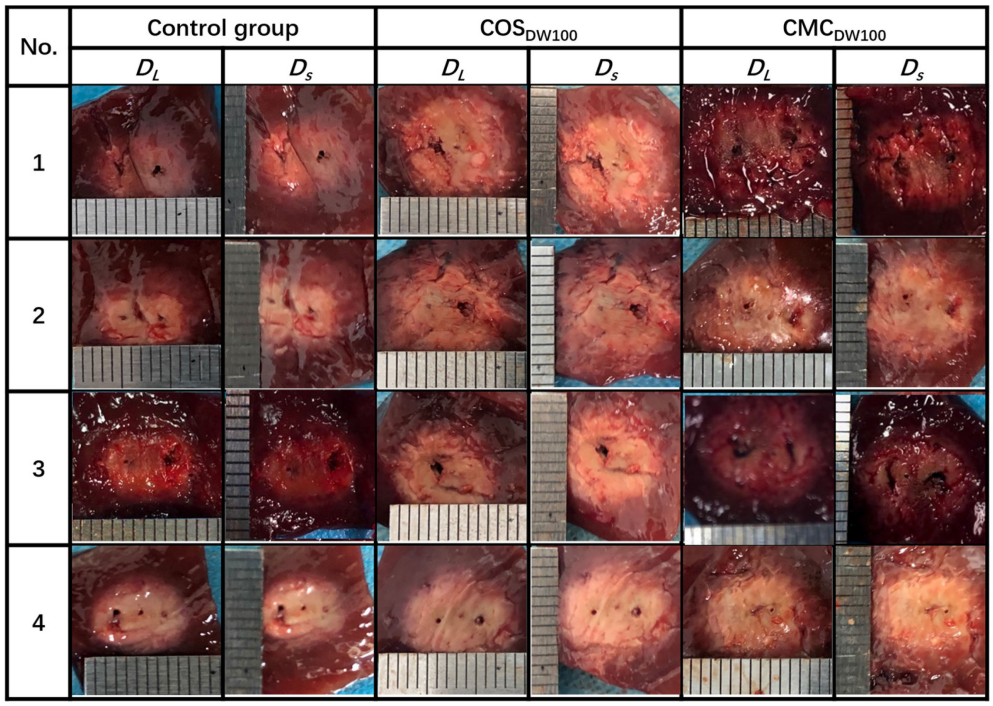

Fig. 8. Images of ablation zones evaluated at the transverse plane for control, COSDW100, and CMCDW100 groups.

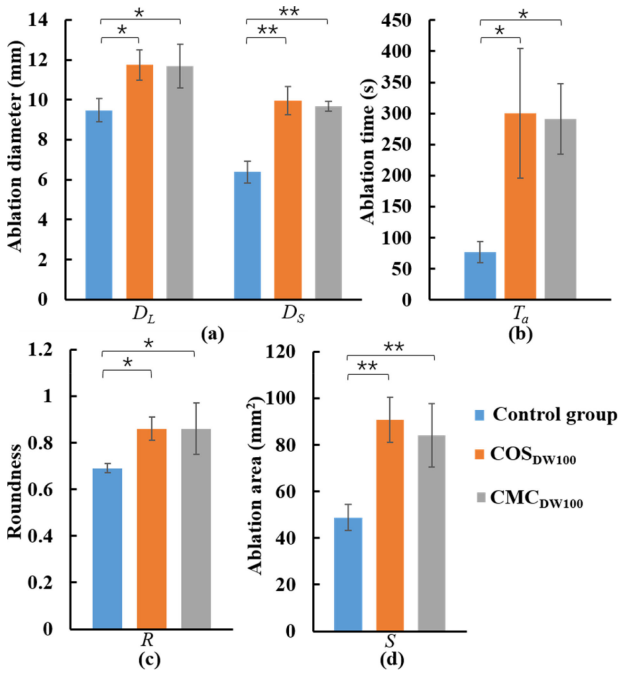

Fig. 9. *In vivo* RFA experiment results: (a) diameter of ablation zones, (b) ablation time, (c) roundness of ablation zones, and (d) area of ablation zones. $^{*}P < 0.05$, $^{**}P < 0.001$.

range of standard deviation of *in vivo* experiment results. Thus, a good agreement in all evaluated indices between the *in vivo* experiment and the computer model was achieved, showing the accuracy of the proposed computer model. Results in both the *in vivo* experiment and the computer simulation showed that the

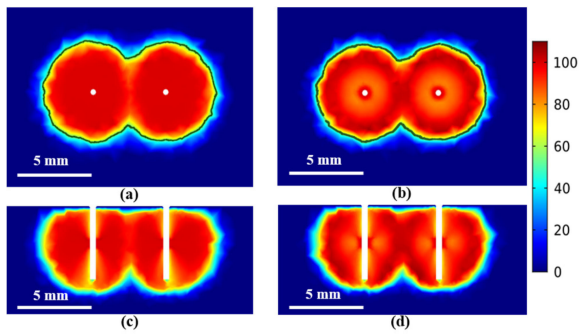

Fig. 10. The solution concentration distributions at the final injection time in the vasculature domain (in mg/mL) for (a) COS$_{DW100}$ and (b) CMC$_{DW100}$ group from the top view, and (c) COS$_{DW100}$ and (d) CMC$_{DW100}$ group from the front view. The black circle represents the isoconcentrate of 50 mg/mL.

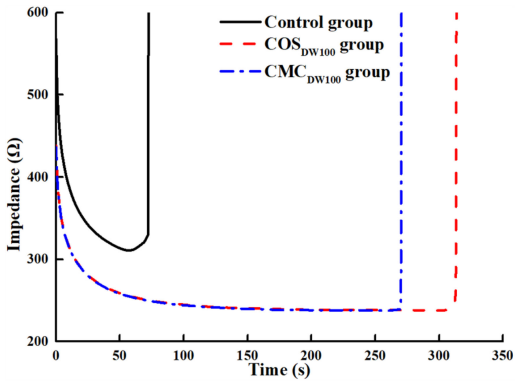

Fig. 11. Impedance changes during the RFA procedures for control, COS$_{DW100}$, and CMC$_{DW100}$ group, respectively.

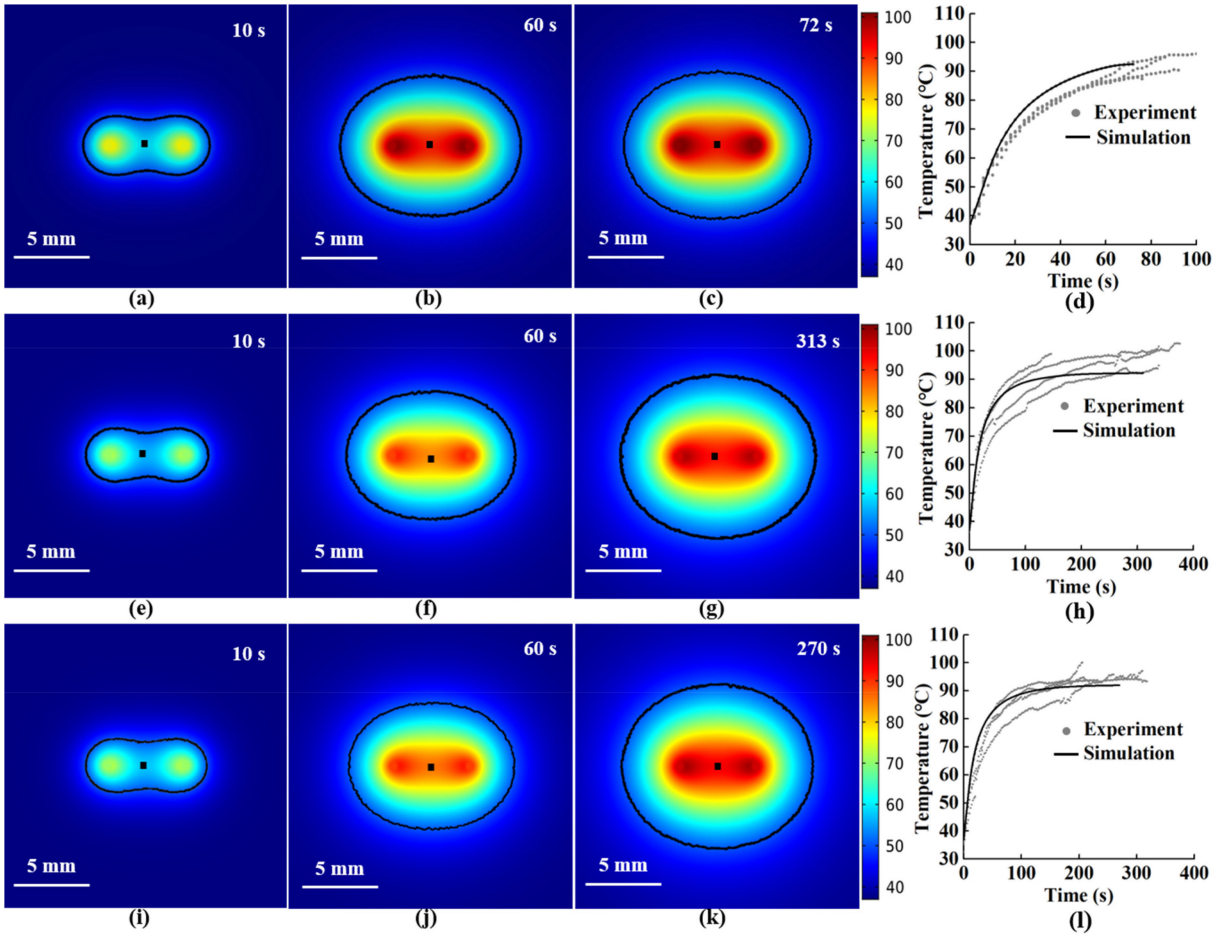

Fig. 12. The temperature distribution (in °C) from top view and the tissue temperature with time at the central point between two electrodes on the transversal plane for (a–d) control group, (e–h) $\mathrm{COS}_{\mathrm{DW100}}$ group, and (i–l) $\mathrm{CMC}_{\mathrm{DW100}}$ group The black circle represents the isotherm of 50 °C, and the black point represents the temperature measurement point.

introduction of $\mathrm{COS}_{\mathrm{DW100}}$ or $\mathrm{CMC}_{\mathrm{DW100}}$ leads to a delay in the roll-off occurrence and improves the temperature distribution, leading to enlargement of the ablation zone in both D_L and D_S, and a rounder ablation zone compared to the situation without cationic solution injection.

V. Discussion

We showed that the injection of cationic polymers was indeed able to modify the electrical conductivity of tissues. Furthermore, the electrical conductivity of cationic polymer solutions can be elevated by an increase in the concentration of cationic polymers (Fig. 6) [14]. In this study, the electrical conductivity of *in vivo* rabbit liver tissues increased as the concentration of cationic polymer, as shown in Fig. 7.

A significant enhancement of ablation zones can be observed using cationic polymer solutions (i.e., $\mathrm{COS}_{\mathrm{DW100}}$ or $\mathrm{CMC}_{\mathrm{DW100}}$) both in the *in vivo* RFA experiment and computer simulation. One of the major reasons is the improvement of electrical conductivity of tissues, which can further improve the following two aspects in the RFA procedure: (1) the ablation time, and (2) the area of heat transfer. With a constant current, a longer ablation time can be achieved in the $\mathrm{COS}_{\mathrm{DW100}}$ or $\mathrm{CMC}_{\mathrm{DW100}}$ group compared to the control group, which means more RF power delivered to tissues. In the computer model, a total of 476 and 414 J of RF power was delivered in the $\mathrm{COS}_{\mathrm{DW100}}$ and $\mathrm{CMC}_{\mathrm{DW100}}$ groups, respectively, compared to the control group of 154 J. The more power deposition during RFA, the larger ablation zone achieved. We also performed RFA experiments with constant power delivery to demonstrate the difference in total power deposition among those three groups, and the similar results are available as Supplementary Fig. 3 accompanying the online article.

The increase in electrical conductivity of tissues around the RF electrode can efficiently decrease the generation of Joule heat around the electrode, which can avoid or delay the roll-off occurrence, and more RF energy can therefore be delivered leading to a larger ablation zone. Note that no significant difference in tissue impedance, temperature distribution, or ablation zone was found between $\mathrm{CMC}_{\mathrm{DW100}}$ and $\mathrm{COS}_{\mathrm{DW100}}$ groups (shown as Fig. 11, Fig. 12e–i, and Fig. 13b–c). This may be due to two competing factors: 1) $\mathrm{COS}_{\mathrm{DW100}}$ has a lower dynamic viscosity, which leads to a larger distribution of cationic polymer solution than $\mathrm{CMC}_{\mathrm{DW100}}$, and 2) $\mathrm{CMC}_{\mathrm{DW100}}$ has a higher electrical conductivity than $\mathrm{COS}_{\mathrm{DW100}}$ in the liver tissues.

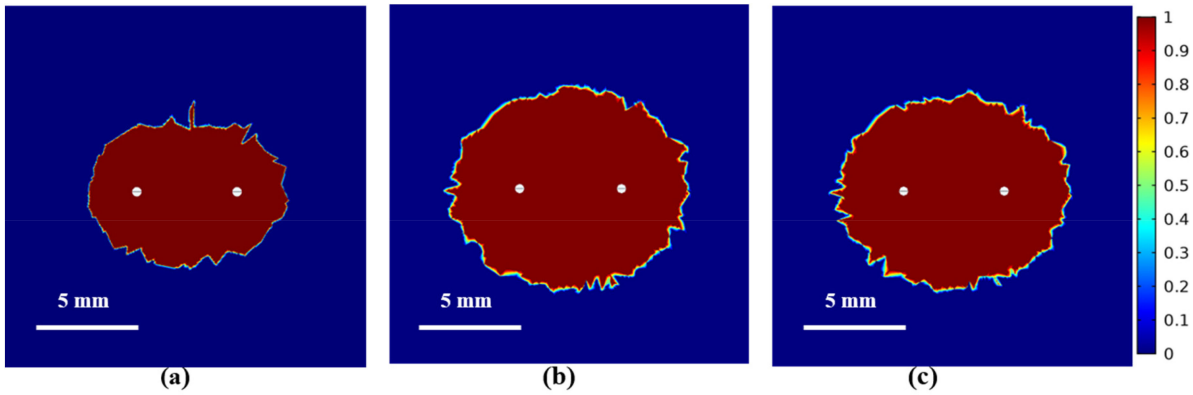

Fig. 13. The tissue death rates of (a) control group, (b) COS_{DW100} group, and (c) CMC_{DW100} group.

TABLE II
In Vivo RABBIT LIVER RADIOFREQUENCY ABLATION RESULTS

ABLATION RESULTS	EXPERIMENT			SIMULATION		
	CONTROL	COS_{DW100}	CMC_{DW100}	CONTROL	COS_{DW100}	CMC_{DW100}
D_L(mm)	9.48±0.57	11.75±0.76	11.68±1.07	9.76	11.50	11.39
D_S(mm)	6.38±0.53	9.95±0.71	9.68±0.24	6.77	9.82	9.47
S(mm^2)	47.6±6.3	92.6±11.5	88.8±9.6	51.9	88.7	84.7
T_a(s)	77±17	300±104	275±73	72	313	270
R	0.67±0.04	0.85±0.05	0.83±0.07	0.69	0.85	0.83

In addition, it is worth mentioning that, different from the saline solution (0.0007 Pa·s in dynamic viscosity), the higher dynamic viscosity of COS_{DW100} (0.01 Pa·s) or CMC_{DW100} (0.61 Pa·s) can limit the solution diffusion area, which may help to avoid large and irregular diffusion zones (see Supplementary Video (3–5)). Therefore, it is reasonable to believe that a regular and predictable ablation zone can be achieved using COS_{DW100} or CMC_{DW100} compared to the saline solution [41], [42]. Besides, in comparison with saline solution, the cationic polymer solutions have additional benefits, including anti-tumor effect, carrier of drug, gene, and protein, and immunostimulatory applications, etc. Thus, a way to combine those organic functions of COS or CMC with RFA merits further study.

Although favorable ablation results were achieved by introducing the cationic polymer solutions to RFA both in the *in vivo* experiment and computer simulation, there are still some limitations to be overcome in the future study.

First, the solution distribution in the liver tissues was only examined by a video camera through the color change of tissues during injection. The solution distribution in the vasculature structures or interstitium was also only investigated by a computer model. Therefore, we believe that it is necessary to further confirm the cationic polymer solution distribution in the liver tissue using a second method.

Second, although only the electrical conductivity of tissues enhanced by the cationic polymer solutions was examined and considered in the computer model, a good agreement in all ablation results (i.e., ablation time, impedance, and ablation zone) was achieved between the *in vivo* experiment and the computer simulation (Table II). However, the enhancing effect on other factors in RFA (e.g., thermal conductivity, the change rate of the electrical or thermal conductivity, etc.) remains to be elucidated with these two cationic polymers.

Third, the size of the electrode used in the study is smaller than the commercial ones used in the clinical practice, and only healthy rabbit liver tissue was studied. Therefore, further studies should be performed using commercial RF systems and large animal tumor models for clinical benefits. An accurate and reliable computer model regarding the real clinical cases would be a great tool to design personalized RFA protocols by optimizing the cationic solution and RFA energy settings.

VI. CONCLUSION

We propose a new way to increase the size of the ablation zone that results from RFA and confirmed the feasibility of this approach using both the *in vivo* experimental and simulation studies. We concluded that, indeed, the performance of RFA can be improved by injecting the cationic polymer solutions into the tissues prior to the application of RF power, mainly by increasing the electrical conductivity of the tissues, thereby delaying the occurrence of "roll-off".

REFERENCES

[1] O. C. Kutlu *et al.*, "Comparative effectiveness of first-line radiofrequency ablation versus surgical resection and transplantation for patients with early hepatocellular carcinoma," *Cancer*, vol. 123, no. 10, pp. 1817–1827, 2017.

[2] D. R. Shah *et al.*, "Current oncologic applications of radiofrequency ablation therapies," *World J. Gastroenterology Oncology*, vol. 5, no. 4, pp. 71–80, 2013.

[3] Z. Fang *et al.*, "Current solutions for the Heat-Sink effect of blood vessels with radiofrequency ablation: A review and future work," in *Advanced Computational Methods in Life System Modeling and Simulation*. Berlin, Germany: Springer, 2017, pp. 113–122.

[4] R. D. Fonseca *et al.*, "Roll off displacement in ex vivo experiments of RF ablation with refrigerated saline solution and refrigerated deionized water," *IEEE Trans. Biomed. Eng.*, vol. 66, no. 5, pp. 1390–1401, May 2019.

[5] B. Zhang *et al.*, "A review of radiofrequency ablation: Large target tissue necrosis and mathematical modelling," *Phys. Med.*, vol. 32, no. 8, pp. 961–971, Aug. 2016.

[6] S. N. Goldberg, "Radiofrequency tumor ablation: Principles and techniques," *Eur. J. Ultrasound*, vol. 13, no. 2, pp. 129–47, Jun. 2001.

[7] Z. Fang *et al.*, "Design of a novel electrode of radiofrequency ablation for large tumors: A finite element study," *J. Eng. Sci. Medical Diagnostics Therapy*, vol. 1, no. 1, 2018, Art. no. 011001.

[8] Z. Fang *et al.*, "Design of a novel electrode of radiofrequency ablation for large tumors: In vitro validation and evaluation," *J. Biomech. Eng.*, vol. 141, no. 3, 2019, Art. no. 031007.

[9] B. Zhang *et al.*, "A new approach to feedback control of radiofrequency ablation systems for large coagulation zones," *Int. J. Hyperthermia*, vol. 33, no. 4, pp. 367–377, 2017.

[10] X.-Y. Jiang *et al.*, "Increasing radiofrequency ablation volumes with the use of internally cooled electrodes and injected hydrochloric acid in ex vivo bovine livers," *Int. J. Hyperthermia*, vol. 35, no. 1, pp. 37–43, 2018.

[11] T.-Q. Zhang *et al.*, "Safety and effect on ablation size of hydrochloric acid-perfused radiofrequency ablation in animal livers," *Int. J. Hyperthermia*, vol. 34, no. 7, pp. 925–933, 2018.

[12] S. N. Goldberg *et al.*, "Radio-frequency thermal ablation with NaCl solution injection: Effect of electrical conductivity on tissue heating and coagulation—Phantom and porcine liver study," *Radiology*, vol. 219, no. 1, pp. 157–165, 2001.

[13] S. K. Kim *et al.*, "CT findings after radiofrequency ablation in rabbit livers: Comparison of internally cooled electrodes, perfusion electrodes, and internally cooled perfusion electrodes," *J. Vascular Interventional Radiol.*, vol. 18, no. 11, pp. 1417–27, Nov. 2007.

[14] N. Mobarak *et al.*, "Conductivity enhancement via chemical modification of chitosan based green polymer electrolyte," *Electrochimica Acta*, vol. 92, pp. 161–167, 2013.

[15] J. B. Marroquin *et al.*, "Chitosan nanocomposite films: Enhanced electrical conductivity, thermal stability, and mechanical properties," *Carbohydrate Polym.*, vol. 92, no. 2, pp. 1783–1791, 2013.

[16] L. Upadhyaya *et al.*, "Biomedical applications of carboxymethyl chitosans," *Carbohydrate Polym.*, vol. 91, no. 1, pp. 452–466, 2013.

[17] B. B. Aam *et al.*, "Production of chitooligosaccharides and their potential applications in medicine," *Mar. Drugs*, vol. 8, no. 5, pp. 1482–1517, 2010.

[18] K.-T. Shen *et al.*, "Inhibitory effects of chitooligosaccharides on tumor growth and metastasis," *Food Chem. Toxicology*, vol. 47, no. 8, pp. 1864–1871, 2009.

[19] Z. Jiang *et al.*, "Preparation and anti-tumor metastasis of carboxymethyl chitosan," *Carbohydrate Polym.*, vol. 125, pp. 53–60, 2015.

[20] F. Liaqat and R. Eltem, "Chitooligosaccharides and their biological activities: A comprehensive review," *Carbohydrate Polym.*, vol. 184, pp. 243–259, 2018.

[21] D. Narayanan *et al.*, "Versatile carboxymethyl chitin and chitosan nanomaterials: A review," *Wires Nanomed. Nanobiotechnology*, vol. 6, no. 6, pp. 574–598, 2014.

[22] M. Ahmed *et al.*, "Image-guided tumor ablation: Standardization of terminology and reporting criteria—A 10-year update," *J. Vascular Interventional Radiol.*, vol. 25, no. 11, pp. 1691–705, Nov. 2014.

[23] F. Avelelas *et al.*, "Antifungal and antioxidant properties of chitosan polymers obtained from nontraditional Polybius Henslowii sources," *Mar. Drugs*, vol. 17, no. 4, 2019, Art. no. 239.

[24] M. E. S. Miranda *et al.*, "Chitosan and N-carboxymethylchitosan: I. The role of N-carboxymethylation of chitosan in the thermal stability and dynamic mechanical properties of its films," *Polym. Int.*, vol. 55, no. 8, pp. 961–969, 2006.

[25] B. Sayın *et al.*, "Mono-N-carboxymethyl chitosan (MCC) and N-trimethyl chitosan (TMC) nanoparticles for non-invasive vaccine delivery," *Int. J. Pharmaceutics*, vol. 363, no. 1/2, pp. 139–148, 2008.

[26] Y.-X. Mei *et al.*, "Protective effect of chitooligosaccharides against cyclophosphamide-induced immunosuppression in mice," *Int. J. Biol. Macromolecules*, vol. 62, pp. 330–335, 2013.

[27] B. Zhang *et al.*, "Tumor ablation enhancement by combining radiofrequency ablation and irreversible electroporation: An in vitro 3D tumor study," *Ann. Biomed. Eng.*, vol. 47, no. 3, pp. 694–705, 2019.

[28] M. L. McHugh, "Multiple comparison analysis testing in ANOVA," *Biochemia Medica*, vol. 21, no. 3, pp. 203–209, 2011.

[29] A. M. Qadri *et al.*, "Effects of saline volume on lesion formation during saline-infused radiofrequency ablation," *Appl. Math. Model.*, vol. 43, pp. 360–371, 2017.

[30] L. T. Baxter and R. K. Jain, "Transport of fluid and macromolecules in tumors. I. Role of interstitial pressure and convection," *Microvasc. Res.*, vol. 37, no. 1, pp. 77–104, 1989.

[31] E. H. Ooi *et al.*, "Comparison between single-and dual-porosity models for fluid transport in predicting lesion volume following saline-infused radiofrequency ablation," *Int. J. Hyperthermia*, vol. 34, no. 8, pp. 1142–1156, 2018.

[32] B. Zhang *et al.*, "Study of the relationship between the target tissue necrosis volume and the target tissue size in liver tumours using two-compartment finite element RFA modelling," *Int. J. Hyperthermia*, vol. 30, no. 8, pp. 593–602, 2014.

[33] M. Jamil and E. Y. Ng, "Quantification of the effect of electrical and thermal parameters on radiofrequency ablation for concentric tumour model of different sizes," *J. Thermal Biol.*, vol. 51, pp. 23–32, Jul. 2015.

[34] J. Valvano *et al.*, "Thermal conductivity and diffusivity of biomaterials measured with self-heated thermistors," *Int. J. Thermophysics*, vol. 6, no. 3, pp. 301–311, 1985.

[35] F. C. Henriques Jr., "Studies of thermal injury: The predictability and the significance of thermally induced rate processes leading to irreversible epidermal injury," *Arch. Pathology (Chic)*, vol. 43, no. 5, pp. 489–502, May 1947.

[36] S. Singh and R. Repaka, "Temperature-controlled radiofrequency ablation of different tissues using two-compartment models," *Int. J. Hyperthermia*, vol. 33, no. 2, pp. 122–134, 2017.

[37] M. Trujillo and E. Berjano, "Review of the mathematical functions used to model the temperature dependence of electrical and thermal conductivities of biological tissue in radiofrequency ablation," *Int. J. Hyperthermia*, vol. 29, no. 6, pp. 590–597, Sep. 2013.

[38] B. Zhang *et al.*, "Numerical analysis of the relationship between the area of target tissue necrosis and the size of target tissue in liver tumours with pulsed radiofrequency ablation," *Int. J. Hyperthermia*, vol. 31, no. 7, pp. 715–725, 2015.

[39] P. D. Richardson and P. G. Withrington, "Liver blood flow: I. Intrinsic and nervous control of liver blood flow," *Gastroenterology*, vol. 81, no. 1, pp. 159–173, 1981.

[40] M. R. Salimpour and E. Shirani, "Heat transfer analysis of skin during thermal therapy using thermal wave equation," *J. Thermal Biol.*, vol. 64, pp. 7–18, 2017.

[41] E. H. Ooi and E. T. Ooi, "Mass transport in biological tissues: comparisons between single-and dual-porosity models in the context of saline-infused radiofrequency ablation," *Appl. Math. Model*, vol. 41, pp. 271–284, 2017.

[42] J. M. Lee *et al.*, "Percutaneous radiofrequency thermal ablation with hypertonic saline injection: In vivo study in a rabbit liver model," *Korean J. Radiol.*, vol. 4, no. 1, pp. 27–34, 2003.